J. Fluid Mech. (2013), *vol.* 715, *pp.* 477–498.
doi:10.1017/jfm.2012.531

Pressure gradient effects on the large-scale structure of turbulent boundary layers

Zambri Harun[1,3], Jason P. Monty[1,†], Romain Mathis[1,2] and Ivan Marusic[1]

[1]Department of Mechanical Engineering, University of Melbourne, Victoria 3010, Australia

[2]Laboratoire de Mécanique de Lille, UMR CNRS 8107, 59655 Villeneuve d'Ascq, France

[3]Department of Mechanical and Materials Engineering, The National University of Malaysia, 43600 Bangi, Malaysia

(Received 10 January 2012; revised 3 October 2012; accepted 23 October 2012)

Research into high-Reynolds-number turbulent boundary layers in recent years has brought about a renewed interest in the larger-scale structures. It is now known that these structures emerge more prominently in the outer region not only due to increased Reynolds number (Metzger & Klewicki, *Phys. Fluids*, vol. 13(3), 2001, pp. 692–701; Hutchins & Marusic, *J. Fluid Mech.*, vol. 579, 2007, pp. 1–28), but also when a boundary layer is exposed to an adverse pressure gradient (Bradshaw, *J. Fluid Mech.*, vol. 29, 1967, pp. 625–645; Lee & Sung, *J. Fluid Mech.*, vol. 639, 2009, pp. 101–131). The latter case has not received as much attention in the literature. As such, this work investigates the modification of the large-scale features of boundary layers subjected to zero, adverse and favourable pressure gradients. It is first shown that the mean velocities, turbulence intensities and turbulence production are significantly different in the outer region across the three cases. Spectral and scale decomposition analyses confirm that the large scales are more energized throughout the entire adverse pressure gradient boundary layer, especially in the outer region. Although more energetic, there is a similar spectral distribution of energy in the wake region, implying the geometrical structure of the outer layer remains universal in all cases. Comparisons are also made of the amplitude modulation of small scales by the large-scale motions for the three pressure gradient cases. The wall-normal location of the zero-crossing of small-scale amplitude modulation is found to increase with increasing pressure gradient, yet this location continues to coincide with the large-scale energetic peak wall-normal location (as has been observed in zero pressure gradient boundary layers). The amplitude modulation effect is found to increase as pressure gradient is increased from favourable to adverse.

Key words: boundary layers, turbulent flows, turbulent boundary layers

1. Introduction

The last decade of wall-turbulence research has seen great progress in the understanding of the large-scale structure of the flow. This was propelled by the investigation of Kim & Adrian (1999) who proposed a model of vortex

† Email address for correspondence: montyjp@unimelb.edu.au

packets to explain the well-known dominance of very-low-frequency energy in the logarithmic region of high-Reynolds-number wall turbulence. Since then, studies of the large-scale structures have shown that they dominate in the log-region and are characterized by alternating regions of low and high momentum (Ganapathisubramani, Longmire & Marusic 2003; del Álamo & Jiménez 2003; Tomkins & Adrian 2003; Ganapathisubramani *et al.* 2005; Hambleton, Hutchins & Marusic 2006). These large-scale events have a typical spanwise width of 0.3–0.5δ, and persist over very long distances, up to 15δ in the streamwise direction (Hutchins & Marusic 2007*a*). They have been interpreted either as long 'trains' of aligned hairpin eddies (Adrian 2007) or as global modes (del Álamo & Jiménez 2006). Importantly, it has been shown that these large-scale structures significantly influence the near-wall region. Abe, Kawamura & Choi (2004) and Hutchins & Marusic (2007*a*) have shown that the large-scale fluctuations of the log-layer are superimposed onto the near-wall small scales, hence imposing a strong 'footprint' at the wall as predicted earlier by the attached eddy hypothesis of Townsend (1976). Indeed, Townsend (1976) suggested that the small-scale structures of the near-wall region should feel all of the wall-parallel motions due to the above attached eddies. Furthermore, the large- and small-scale interaction is not only a linear superposition; it has been observed that the large-scale features that inhabit the log-region appear to amplitude modulate the smaller motions near the wall (Hutchins & Marusic 2007*b*; Nikora *et al.* 2007). Previous studies have also suggested such a coupling (Rao, Narasimha & Badri Narayanan 1971; Bandyopadhyay & Hussain 1984; Grinvald & Nikora 1988). A clear modulation effect has been supported recently by the study of Mathis, Hutchins & Marusic (2009*a*) who quantified the degree of amplitude modulation. It should be noted that both effects, superposition and modulation, have been found to increase as the Reynolds number increases (Hutchins & Marusic 2007*a*; Mathis *et al.* 2009*a*). This is due to an increase in large-scale activity with Reynolds number (Hutchins & Marusic 2007*a*,*b*; Marusic, Mathis & Hutchins 2010).

The general presence and qualitative form of these large-scale features appears to be a recurrent property of wall-bounded flows, including internal flows (Monty *et al.* 2007; Balakumar & Adrian 2007; Bailey *et al.* 2008), and the atmospheric surface layer (Kunkel & Marusic 2006; Marusic & Heuer 2007; Marusic & Hutchins 2007). Furthermore, recent studies comparing the flow structure in boundary layer, pipe and channel flows at matched Reynolds number have shown similar small- and large-scale interaction in all flows (Monty *et al.* 2009; Mathis *et al.* 2009*b*), despite the apparent difference in large-scale phenomena (Kim & Adrian 1999). Hence, it is logical to consider what interaction these large-scale log-region motions have in flows subjected to a pressure gradient.

A survey of the literature reveals many studies dealing with pressure gradient effects in turbulent boundary layers, but most of them have focused only on statistical properties (see Jones & Launder 1972; Nagano, Tagawa & Tsuji 1992; Spalart & Watmuff 1993; Krogstad & Skåre 1995; Marusic 1995; Fernholz & Warnack 1998; Jones, Marusic & Perry 2001; Skote & Henningson 2002; Nagib & Chauhan 2008; Bourassa & Thomas 2009, among others) and little is known about coherent structures. The first clues were given decades ago in the work of Bradshaw (1967*b*) on the flow structure of equilibrium boundary layers in adverse pressure gradient (APG) flows. From measurements made in three boundary layers, one with zero pressure gradient (ZPG) and two with APG (moderate and strong), Bradshaw (1967*b*) identified some important features of wall-bounded flows subjected to an increasing pressure gradient. Specifically, he showed a strengthening and rising influence on the flow of the large

eddy motions as the pressure gradient increased. From a spectral analysis, he observed a rise of the low-frequency energetic content in the outer region. He suggested that the large scales can be crudely regarded as universal, differing only by scale factors of velocity and length. Because the large eddies contribute significantly to the local shear stress, and hence the turbulence production, Bradshaw (1967*b*) speculated that they should control the energy supply to the smaller scales in the outer part of a boundary layer. This was also confirmed by Dengel & Fernholz (1990) and Skåre & Krogstad (1994) in strong APG flows, where a secondary peak in turbulence production was observed in the outer region. However, such structures appear not to change the universality of the smaller motions in the inner layer, which led Bradshaw (1967*b*) to reiterate previous observations that the large-scale motions are mostly 'inactive'. Recalling that, in the inner layer, an 'active' universal component contributes largely to the shear stress, an 'inactive' component (imposed by the eddies and pressure fluctuations in the outer layer) does not produce shear stress and can be regarded as a quasi-steady oscillation of the inner-layer flow (Townsend 1961; Bradshaw 1967*a*). However, the inactive motions, being larger swirling and meandering eddies, produce shear stress in the outer region (Townsend 1976). It should be acknowledged that the conclusions of Bradshaw (1967*b*) were remarkably insightful given the limited data available at the time.

Advances in numerical simulation capability have enabled deeper analysis of the flow structure of turbulent boundary layers. Direct numerical simulation (DNS) studies carried out on turbulent boundary layers near separation (Spalart & Coleman 1997; Na & Moin 1998; Skote & Henningson 2002) or in equilibrium (Lee & Sung 2009), have shown that under a strong APG, the near-wall streaks are significantly weakened with wider spanwise spacing. However, these studies have provided information only about the turbulent structure of the near-wall region, and at very low Reynolds numbers in which the log-region is limited or non-existent. It is only very recently that large-scale outer-region motions have received more attention (Dixit & Ramesh 2010; Monty, Harun & Marusic 2011; Rahgozar & Maciel 2011). From a study of the cross-correlation between wall shear stress and velocity fluctuations in reverse-transitional flow, Dixit & Ramesh (2010) have shown a considerable elongation of the large scales with a smaller structure inclination angle as FPG strength increases. Conversely, Krogstad & Skåre (1995) have previously shown that large-scale structures were shortened and structure inclination angle increased in APG flow. The thickening or flattening of these structures identified by Dixit & Ramesh (2010) and Krogstad & Skåre (1995) are difficult to measure as they are primarily inferences from superimposed contour lines. Rahgozar & Maciel (2011) studied the large-scale features in the outer region of a turbulent boundary layer subjected to a strong APG. They identified large and long meandering streaky patterns, similar to those observed in ZPG flows (Hutchins & Marusic 2007*a*). Furthermore, they noted that these events appear less frequently than in the canonical case. Overall, one of the issues in pressure gradient flows is that the number of parameters known to affect the flow is considerably larger than in ZPG boundary layers. In an attempt to reduce the parameter space, and enhance our understanding on pressure-gradient effects, Monty *et al.* (2011) performed a parametric study on the effects of increasing APG in constant conditions (matched Reynolds number and constant viscous scaled sensor length). Unlike previous studies, they have studied the energy content of the flow, and found that the large-scale log-region events are strongly energized by the increasing pressure gradient, becoming a significant contributor to the increasing streamwise turbulent intensity profile across the boundary layer.

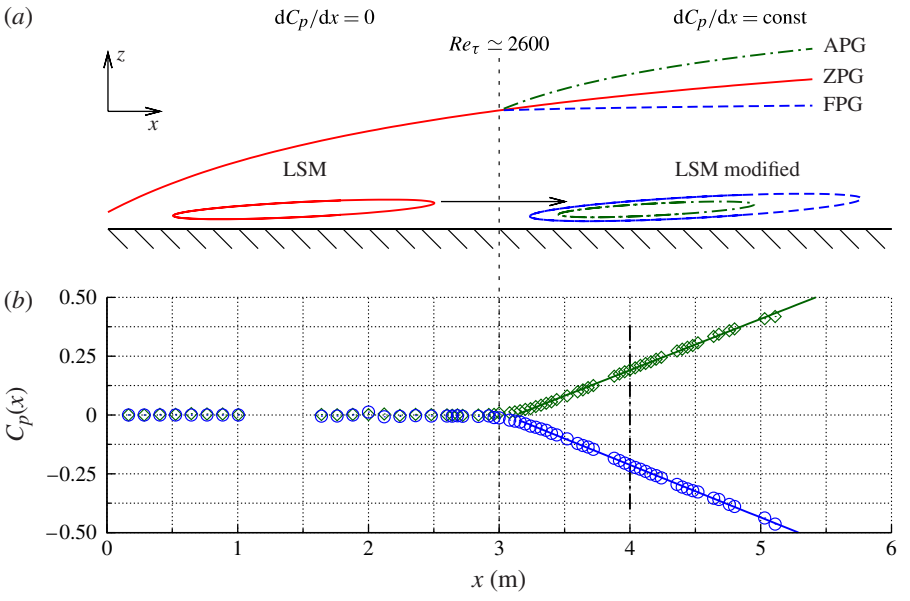

FIGURE 1. (Colour online) (*a*) Illustration of turbulent boundary layer subjected to a change in pressure gradient (LSM: large-scale motions); (*b*) pressure coefficient C_p, for: ◊, APG; and ○, FPG. Solid lines indicate a linear fit of C_p and the vertical dash–dotted line indicates the measurement location for data presented in this paper.

Following on from the observation that the large-scale features have a strong influence in wall-bounded flows, this paper aims to understand the change in the large-scale structures and their interaction with small scales when a mild pressure gradient is imposed. Similar to Monty *et al.* (2009) and Mathis *et al.* (2009*a*) this investigation is undertaken through a comparison of boundary layers with carefully matched Reynolds number and measurement conditions. Hence, we consider three pressure gradient flows, favourable pressure gradient (FPG), ZPG and APG, which nominally have the same initial conditions, i.e. a ZPG turbulent boundary layer at $Re_\tau \simeq 2600$ ($\pm 10\,\%$) as illustrated in figure 1(*a*). For this purpose, two new experiments carried out in boundary layers with APG and FPG are presented and compared with the ZPG case documented in Monty *et al.* (2009) and used by Mathis *et al.* (2009*a*). The data analysis will only consider scaling with variables appropriate for ZPG boundary layers. This approach is necessary since the aim is to identify changes to flow characteristics due to a mild pressure gradient, relative to the ZPG case, for a fixed range of scales defined by $Re_\tau = \delta U_\tau/\nu \approx 3100$.

2. Experimental details

The experiments were performed in an open-return blower wind tunnel. The tunnel has a settling chamber containing honeycomb and five screens, followed by a contraction with area ratio of 8.9:1, leading into a fixed ceiling, ZPG inlet section 1.2 m long and a cross-sectional area of 940 mm × 375 mm (a trip wire is placed at the start of this section). The inlet is followed by a 4.2 m test section with an adjustable ceiling made from acrylic and hung by threaded rods such that its height is easily adjusted. However, due to the requirement that the ceiling be adjustable and the

fact that the string holding the measurement probe protrudes through the ceiling, there is a restricted number of streamwise locations where measurements can be undertaken (typically every 0.5 m from the inlet). In both pressure gradient cases considered, the free stream turbulence level remains below 1 % and the boundary layer thickness is less than 20 % of the tunnel height to ensure that the boundary layer and the ceiling do not influence each other. Further details of the wind tunnel can be found in Monty *et al.* (2011) and Marusic (1995). The ZPG case was performed in the high-Reynolds-number boundary layer wind tunnel (HRNBLWT) at Melbourne (Nickels *et al.* 2005). The choice of using the HRNBLWT instead of the pressure-gradient wind tunnel for the ZPG case has been made for two reasons: (i) the HRNBLWT is among the highest-quality ZPG flows that can be achieved in a laboratory; (ii) ZPG data taken in the pressure-gradient tunnel was only taken for validation purposes in the early stages of the measurement program (of which a small subset of the data is reported here) and did not have the same level of tolerance on measurement parameters or experimental error as the non-ZPG cases.

2.1. *Pressure gradient and experimental parameters*

The pressure coefficient for an incompressible fluid is given by

$$C_p = \frac{P - P_\infty}{\frac{1}{2}\rho {U_\infty}^2} = 1 - \left(\frac{U_1}{U_\infty}\right)^2, \tag{2.1}$$

where P is the local static pressure, P_∞ is the static pressure at the beginning of the inlet section ($x = 0$ m) and U_1 and U_∞ are the local and inlet free stream velocities, respectively. Figure 1(*b*) shows the C_p distribution for the APG and FPG cases. The test section is configured such that a ZPG ($C_p = 0 \pm 0.01$) is maintained until $x \approx 3$ m, from which point a constant pressure gradient is maintained for both non-ZPG cases.

Measurements from three boundary layers subjected to different pressure gradients were acquired at a matched friction Reynolds number $Re_\tau \approx 3000$. The friction Reynolds number is defined as $Re_\tau = \delta U_\tau/\nu$, where δ is the boundary layer thickness determined by the method of Jones *et al.* (2001), U_τ is the friction velocity described in § 2.2 and ν is the kinematic viscosity. It should be noted that the three flows have a similar initial condition, $Re_\tau \simeq 2600$ at the upstream transition from ZPG to FPG/APG ($x \approx 3$ m) as illustrated in figure 1(*a*). All of the measurements were performed using single hot-wire anemometry. Wollaston wires were soldered to the prong tips and etched to give a platinum filament of the desired length l. Filament diameters of $\phi = 2.5$ μm (APG/FPG) or $\phi = 5$ μm (ZPG) were used. In an attempt to avoid variations due to spatial resolution effects (see Hutchins *et al.* 2009) when comparing the different pressure gradient flows, a non-dimensional hot-wire length of $l^+ \simeq 30$ was maintained ($l^+ = lU_\tau/\nu$). The non-dimensionalized sampling duration has been kept sufficiently large, $TU_1/\delta > 20\,000$, where T is the total sampling duration at each height in seconds. A summary of the experimental conditions are given in table 1. The error in hot-wire measured mean velocity is estimated at ±1 % and turbulence intensity ±2 % (as determined by Hutchins *et al.* 2009; Monty *et al.* 2009, and others).

The pressure gradient in boundary layer flows can be characterized by a variety of non-dimensional parameters. In this paper, the Clauser pressure gradient parameter β, the acceleration parameter K and the viscous-scaled pressure gradient p_x^+ are reported:

$$\beta = \frac{\delta^*}{\tau_w}\frac{\mathrm{d}P}{\mathrm{d}x}, \quad K = \frac{\nu}{{U_1}^2}\frac{\mathrm{d}U_1}{\mathrm{d}x}, \quad p_x^+ = \frac{\nu}{\rho U_\tau^3}\frac{\mathrm{d}P}{\mathrm{d}x}, \tag{2.2}$$

PG	Symbols	x (m)	Re_τ	Re_θ	U_1 (m s^{-1})	U_∞ (m s^{-1})	U_τ (m s^{-1})	δ (mm)	l^+	t^+	β $\times 10^7$	K $\times 10^{-3}$	P_x^+
APG	◊	4.0	3200	12 030	20.0	22.3	0.645	77	31.2	0.52	1.74	−1.05	3.1
ZPG	□	5.0	3020	8160	12.5	12.5	0.457	100	30.0	0.57	0	0	0
FPG	○	4.0	3100	6450	18.1	16.5	0.710	66	30.5	0.67	−0.42	0.77	−1.3

TABLE 1. Experimental parameters. Here $t^+ = U_\tau^2/(f_s\nu)$ is the non-dimensionalized time, where f_s is the sampling frequency.

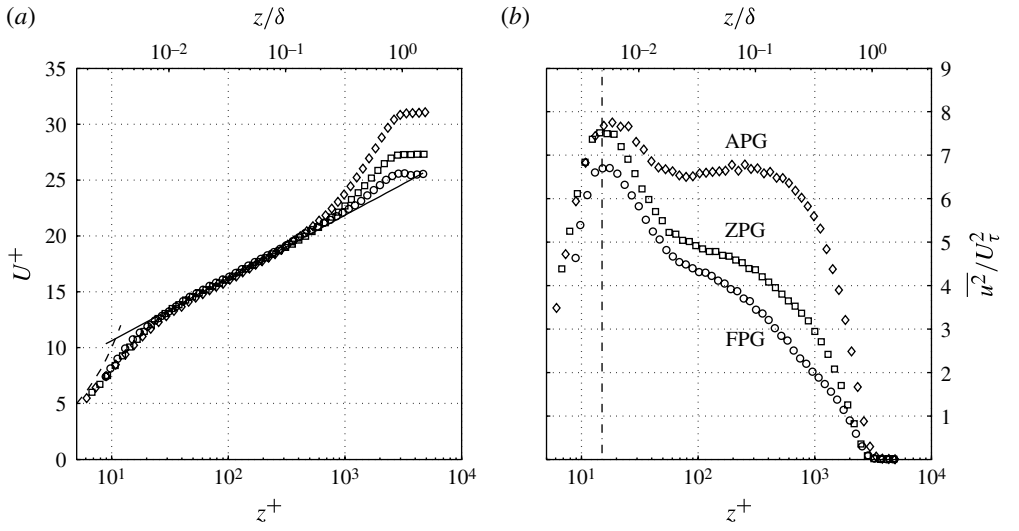

FIGURE 2. Comparison of the three boundary layer measurements at matched Reynolds number, $Re_\tau \approx 3000$; (*a*) mean velocity profiles U^+; and (*b*) broadband turbulence intensity profiles $\overline{u^2}/{U_\tau}^2$: ◇, APG; □, ZPG; and ○, FPG. The solid line in plot (*a*) shows $U^+ = \kappa^{-1}\log(z^+) + A$ ($\kappa = 0.41$, $A = 5.0$), and the dashed line shows $U^+ = z^+$. The dash–dotted line in (*b*) indicates $z^+ = 15$.

where δ^* is the displacement thickness. Table 1 shows that the parameter values are of similar magnitudes for the APG and FPG boundary layers and that the pressure gradients are relatively mild. This was desired such that the flows maintained some degree of universality; namely, Prandtl's law of the wall holds for all cases and some logarithmic region of the mean velocity profile exists.

2.2. *Skin friction*

Oil-film interferometry (OFI) has been used to independently determine the friction velocity, $U_\tau = \sqrt{\tau_w/\rho}$, for all boundary layer measurements (where τ_w is the mean wall shear stress and ρ is the fluid density). This technique allows us to determine U_τ within $\pm 1\,\%$ of error. Details of the OFI technique, analysis method and error estimation are available in Chauhan, Ng & Marusic (2010).

3. Results

3.1. *Mean velocity and turbulence intensity profiles*

Figure 2(*a*) shows the mean velocity profile scaled with inner variables ($U^+ = U/U_\tau$, $z^+ = zU_\tau/\nu$) for all three pressure gradient flows. Two notable features can be observed. First, all profiles collapse within experimental error in the inner region ($z \lesssim 0.1\delta$). This characteristic was expected due to the mild magnitude of the pressure gradients imposed. It has been shown in stronger pressure gradient flows that a deviation of the mean velocity profile from the classical log-law can occur (Krogstad & Skåre 1995; Nagano, Tsuji & Houra 1998; Nagib & Chauhan 2008; Monty *et al.* 2011). The second noticeable feature is the consistent increase of the mean velocity relative to U_τ in the wake region with pressure gradient (Nagano *et al.* 1992; Krogstad & Skåre 1995; Skote & Henningson 2002; Nagib & Chauhan 2008; Monty *et al.*

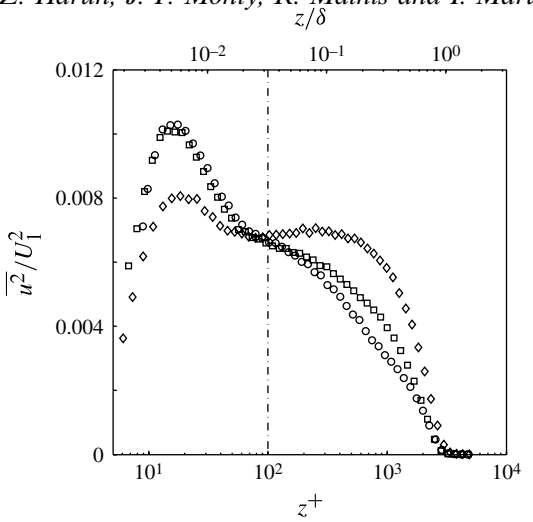

FIGURE 3. Broadband turbulent intensity profiles for FPG, ZPG and APG data at $Re_\tau \approx 3000$ scaled with local free stream velocity, U_1. The dash–dotted line indicates $z^+ = 100$. For symbols, refer to table 1.

2011, among others). The corresponding broadband turbulence intensity profiles are displayed in figure 2(*b*). We recall that the non-dimensional sensor size l^+ and the Reynolds number are nominally equal for all flows. Clearly, there is no similarity in $\overline{u^2}/U_\tau^2$. As the pressure gradient increases, the turbulence intensity scaled with friction velocity rises significantly all of the way through the boundary layer. The difference is not a simple scaling problem since the distributions are very different in shape. The main discrepancies appear in the outer region where it can be observed that the turbulence intensity drops rapidly with wall distance in the FPG boundary layer. However, in the APG flow, a weak secondary peak is observed. At this point, we conclude only that the boundary layer is more energetic relative to the wall-friction loss as the pressure gradient changes from favourable to adverse, and particularly so in the outer region. A scale-based explanation for this observation will be given in § 3.4 using a scale-decomposition analysis.

To demonstrate that the rise in energy in the outer region is not due simply to a scaling argument, the turbulence intensity profiles have been plotted scaled with U_1 in figure 3. In the near-wall region, the intensity is now lowest in the APG case and increases as the pressure gradient changes sign. However, scaling with U_1 in the near-wall region is not appropriate since U_1 is not a relevant velocity scale so far from the free stream. In figure 3, the vertical dash–dotted line indicates $z^+ = 100$, if we consider the outer region taken from this line towards the edge of the boundary layer, the intensity still clearly rises with pressure gradient.

3.2. *Turbulence production*

To understand the mechanics behind the rise of the turbulence energy from FPG to APG, we analyse turbulence production for each flow. The general equation for turbulence production is given by

$$P = -\overline{u_i u_j}\,\overline{S_{ij}}, \quad \overline{S_{ij}} = \frac{1}{2}\left(\frac{\partial U_i}{\partial x_j} + \frac{\partial U_j}{\partial x_i}\right), \tag{3.1}$$

where u_i are the fluctuating velocity components, $\overline{S_{ij}}$ is the rate of strain tensor and U_i is the mean velocity component (Pope 2000). In wall-bounded flows, the mean spanwise velocity is zero, which reduces the general equation considerably so that the turbulence production, P^+ scaled with inner variables, can be written as

$$P^+ = -\overline{uw}^+ \frac{\partial U^+}{\partial z^+} - \overline{u^2}^+ \frac{\partial U_1^+}{\partial x^+} + \overline{w^2}^+ \frac{\partial U_1^+}{\partial x^+} - \overline{uw}^+ \frac{\partial W^+}{\partial x^+}. \tag{3.2}$$

where w is the wall-normal velocity fluctuation. Since all experiments performed in this study used only single hot-wire sensors, w was not measured. To acquire this data, a two-component measurement is required, using an X-wire or similar, and this is challenging due to spatial resolution issues and accessing the near-wall region in our flow. To proceed, however, it is sufficient to accept $\overline{w^2}^+$ is $O(1)$ for all wall distances in the energy containing region, i.e. $1 < z^+ < \delta^+$ (Kunkel & Marusic 2006). It is instructive to consider the orders of magnitude of each term in (3.2): the first term, $-\overline{uw}^+ \partial U^+/\partial z^+$, is O($10^{-1}$), while $-\overline{u^2}^+ \partial U_1^+/\partial x^+$ and $\overline{w^2}^+ \partial U_1^+/\partial x^+$ are O(10^{-4}), and $-\overline{uw}^+ \partial W^+/\partial x^+$ is O(10^{-6}); thus, the second, third and fourth terms are negligible.

Figure 4(*a*) shows the Reynolds shear stress, $\overline{uw}^+$ profiles for each pressure gradient. Although no w measurements were made, reasonable estimates for $\overline{uw}^+$ can be obtained in flows that are two-dimensional in the mean using an integrated version of the mean momentum equation, and here we use the formulations described by Perry, Marusic & Li (1994) and Perry, Marusic & Jones (2002). Here, an analytical expression for the total shear stress is obtained by using a law of the wall/wake formulation and the continuity equation and integrating the mean momentum equation. Marusic (1995) showed detailed comparisons between the Perry *et al.*formulations and high-fidelity flying X-wire measurements to confirm the validity of the approach. Given that the data in figure 4(*a*) is estimated, we simply note here that the APG case has much higher $\overline{uw}^+$ magnitude, while the $\overline{uw}^+$ profile in the FPG case is only slightly lower than the ZPG case. It is certainly the outer region that distinguishes the three pressure gradient cases as earlier observed in the streamwise turbulence intensity profiles. The increased Reynolds shear stress trend in the outer region is well in agreement with the increasingly APG data of Bradshaw (1967*b*), Nagano *et al.* (1992) and Lee & Sung (2009). Conversely, a decrease in Reynolds shear stress in the outer region has been reported with increasingly favourable pressure gradient (Jones *et al.* 2001).

The estimated turbulence production, P^+, is shown in figure 4(*b*). Turbulence production is locally highest in the near-wall region as shown by experimental and numerical studies. These observations led Robinson (1991) to summarize that the thin, near-wall buffer region is the most important zone of the boundary layer in terms of the production of turbulence energy. Figure 4(*b*) also shows that there is almost no observable change across the three pressure gradient cases in this region. This is in agreement with DeGraaff & Eaton (2000) who found that P^+ collapses across all acceleration parameters except for the lowest-Reynolds-number data (which they attribute to low-Reynolds-number effects). In contrast, previous FPG studies have shown that a high acceleration parameter acts to reduce turbulence production in the near-wall region (Fernholz & Warnack 1998; Bourassa & Thomas 2009). Skote, Henningson & Henkes (1998) found that P^+ increases in flows subjected to an APG. Most of the contradictory studies, however, consider strong pressure gradients and low Reynolds numbers. The combination of these parameters results in much larger values of $\partial U_1^+/\partial x^+$ than that considered in the present investigation. For example, in Nagano

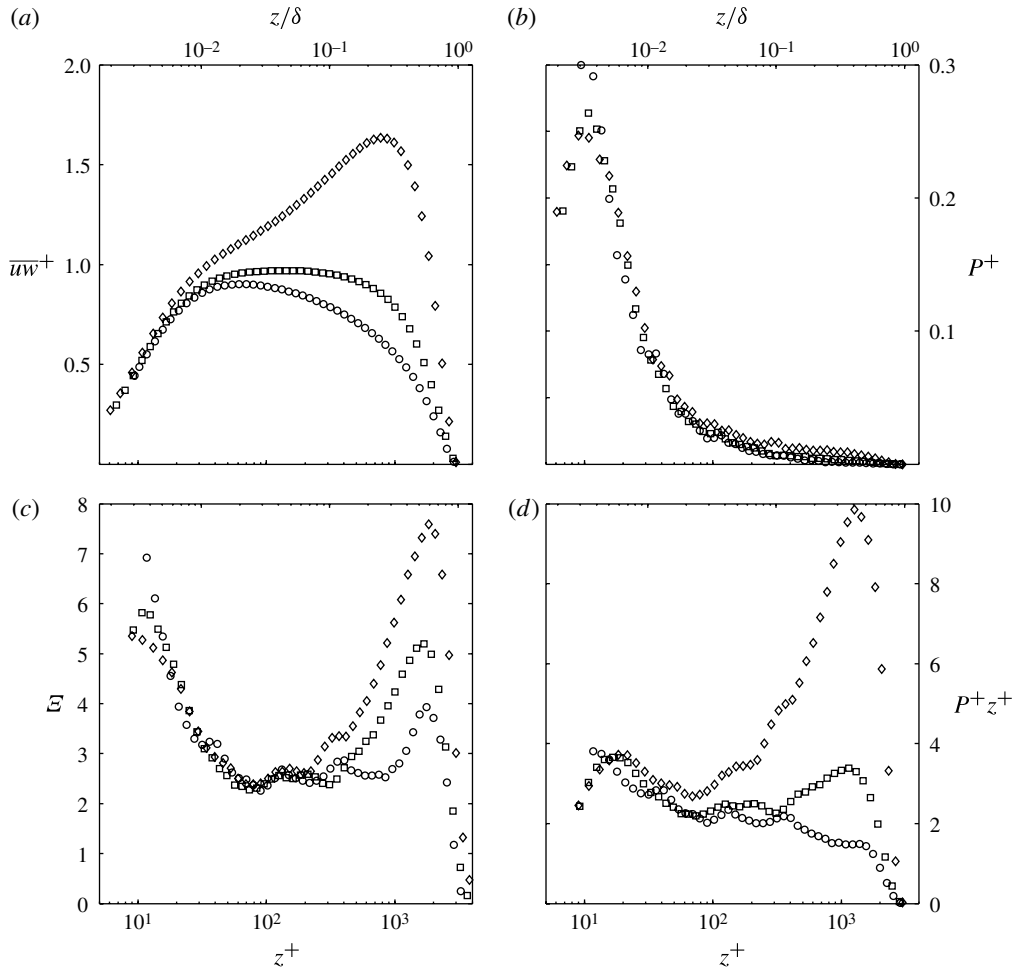

FIGURE 4. Profiles of (*a*) Reynolds shear stress, $\overline{uw}^+$ (using the formulation of Perry *et al.* (2002), based on the integrated momentum equation), (*b*) estimated turbulence production, P^+, (*c*) diagnostic function, Ξ, and (*d*) pre-multiplied turbulence production, P^+z^+: ◇, APG; □, ZPG; and ○, FPG.

et al. (1998) the strong APG has $\partial U_1^+/\partial x^+$ five times larger than in our APG case, while this quantity in the investigation of Bourassa & Thomas (2009) is one order of magnitude larger than our FPG case (for their $x/L = 0.25$, strong FPG case).

In the outer region, it is not clear how P^+ changes since its magnitude is low relative to the inner region. Although one can observe a slightly elevated production for the APG case in figure 4(*b*), nothing further can be concluded from this representation. Previous work indicates that there is a general increase of outer layer production as the pressure gradient varies from favourable to adverse (Nagano *et al.* 1992; Skåre & Krogstad 1994; Fernholz & Warnack 1998; Skote *et al.* 1998; Aubertine & Eaton 2005). It is noted that Nagano *et al.* (1992) and Skåre & Krogstad (1994) have used outer scaling when presenting production statistics, however an increase (with pressure gradient) in the outer region in those studies is still observed if

inner scaling is used. Since the choice of inner or outer scaling does not change the conclusions, the remaining discussion is based on inner-scaled quantities.

Marusic *et al.* (2010) has shown that the P^+ representation of figure 4(*b*) visually underestimates the importance of the contribution in the log-region when using semi-logarithmic axes. Instead, Marusic *et al.* propose that one should plot P^+z^+ on such a graph since the total production can be written as

$$P^+_{tot} = \int_0^{\delta^+} P^+ \,\mathrm{d}z^+ = \int_0^{\delta^+} P^+z^+ \,\mathrm{d}(\log z^+). \tag{3.3}$$

Therefore, on a plot of P^+z^+ versus $\log z^+$, equal areas of the plot represent equal contributions to the total production. In ZPG or in mild pressure gradient cases where the second and third terms in (3.2) can be neglected, the contribution to the bulk production can be written as

$$P^+z^+ = -\overline{uw}^+ \frac{\partial U^+}{\partial z^+} z^+ = -\overline{uw}^+ \Xi. \tag{3.4}$$

It is now seen that the premultiplied form of the production is simply the Reynolds shear stress, $-\overline{uw}^+$ multiplied by the diagnostic function, $\Xi = z^+\partial U^+/\partial z^+$. The diagnostic function profiles for all pressure gradient cases are shown in figure 4(*c*) and the premultiplied turbulence production P^+z^+ profiles are shown in figure 4(*d*). It can be observed from the velocity profiles in figure 2(*a*) that the inflection in the wake of the velocity profile causes a peak in Ξ in the outer region. This peak, combined with the outer peak in $\overline{uw}^+$, gives a large contribution to P^+z^+ in the outer region; the APG case, therefore, exhibits the largest P^+z^+, followed by the ZPG and FPG cases.

In the near-wall region, P^+z^+ is observed to be almost invariant with pressure gradient. The reason for this invariance can be explained as follows. Here Ξ will not change with pressure gradient near the wall, as long as Prandtl's law of the wall holds (which is the case for mild pressure gradients such as those considered here). Further, the Reynolds shear stress near the wall does not change significantly for mild pressure gradient strengths. To understand this, consider the two main contributors to the near-wall motions; small scales of the near-wall cycle and the 'foot-print' of the large scales which act to modulate the small scales. The large-scale structure itself does not contribute directly to $\overline{uw}^+$ near the wall (in contrast to $\overline{u^2}^+$). It will be shown in § 3.3 that there is considerably more energy in the large scales in the APG flow, but much less change in the small scales near the wall. As such, the small scales may experience more or less modulation with pressure gradient, however, the mean $\overline{uw}^+$ is insensitive to the pressure gradient. This is in agreement with the aforementioned observations of Townsend (1976) and Bradshaw (1967*a*) who concluded that the larger-scale motions of the outer layer are mostly inactive, in the sense that they are not contributing to the shear stress near the wall despite their significant local contribution in the outer region.

The statistical analyses presented thus far indicate that it is the outer region that contains the distinguishing features for the three pressure gradient cases. Since large-scale features are associated with this region (Adrian, Meinhart & Tomkins 2000; Hutchins & Marusic 2007*a*), it is important to understand how pressure gradient causes certain features to be more energized (or attenuated). The following sections attempt to provide some insight into the structure of the flow that contributes to the observed statistical behaviours.

3.3. *Energy spectra*

The energy distribution of ZPG turbulent boundary layers has previously been studied in detail by Hutchins & Marusic (2007*a*,*b*) and Balakumar & Adrian (2007) and others. Such studies have also been well documented in channel and pipe flows (del Álamo *et al.* 2004; Monty *et al.* 2009). Monty *et al.* (2009) provided a direct comparison of the energy distribution between a turbulent boundary layer (ZPG), channel and pipe flow, at matched Reynolds number, highlighting similarities and noticeable differences in the large-scale content. A similar comparison of three turbulent flows is presented here.

Figure 5(*a–c*) shows spectragrams (Hutchins & Marusic 2007*b*) for all three flows, where contours of the premultiplied power spectral density ($k_x\phi_{uu}/U_\tau^2$) are plotted against wall distance z^+ and non-dimensional wavelength λ_x^+. Here $k_x = 2\pi f/U_c$ is the wavenumber and U_c is the convection velocity taken to be the local mean velocity (invoking Taylor's frozen turbulence hypothesis). The overall shape of the three maps are seen to be similar, however, there are substantial differences appearing in the outer region. For all of the maps, a similar highly energetic peak can be observed near the wall at $z^+ \approx 15$, centred around $\lambda_x^+ \approx 1000$ (marked by the symbol '+'). This peak, referred to as the 'inner peak', is the well-known energetic signature of the near-wall cycle of elongated and quasi-streamwise streaks (Kline *et al.* 1967). As the distance from the wall increases, the emergence of a secondary peak or a ridge can be seen (vertical dash–dotted line), which is especially evident for the APG boundary layer. This peak, referred to as the 'outer peak', corresponds to the signature of the largest-scale motions or superstructures (Hutchins & Marusic 2007*a*). The wall-normal location of the outer peak in ZPG boundary layers has been reported by Mathis *et al.* (2009*a*) to be Reynolds number dependent, and situated at the geometrical centre of the log-layer, $z^+ = 3.9Re_\tau^{1/2}$. In cases of FPG and APG, it is quite clear that this outer peak does not occur at the same location as in the ZPG case ($z^+ = 3.9Re_\tau^{1/2} \approx 200$). The existence of the outer peak is much clearer for the APG boundary layer, whereas it is very weak for the FPG case. This suggests that one of the effects of the APG is to strengthen and/or increase the population of large-scale motions. The outer peak has been observed previously in ZPG turbulent boundary layers to emerge around $\lambda_x \approx 6\delta$ (Hutchins & Marusic 2007*a*; Mathis *et al.* 2009*a*; Monty *et al.* 2009). A similar length scale is observed for FPG and APG, suggesting that similar types of structures inhabit the log-region in each flow.

From the overall picture of the energy content of the three flows, given in figure 5(*a–c*), it is evident that the most significant differences appear in the outer part of the boundary layer, although there is some discrepancy remaining close to the wall (more evident in the total streamwise energy plot of figure 2(*b*). The difference between flows is particularly noticeable in figures 5(*d*) and 5(*e*), in which the energy map of the ZPG boundary layer has been subtracted from the APG and FPG maps, respectively. It is observed that a significant amount of energy is added in the outer region for the APG flow, and conversely missing from the FPG layer. Interestingly, the peak energy difference occurs at approximately the same location $z/\delta \approx 0.2$–0.3 and the same wavelength $\lambda_x/\delta \approx 2$–$3$ for both APG and FPG cases.

To interrogate the energy distribution in more detail, the energy spectra from four selected wall-normal locations are plotted in figure 6. The wall-normal locations chosen are: (*a*) $z^+ \approx 15$, (*b*) $z^+ \approx 100$, (*c*) $z^+ \approx 3.9Re_\tau^{1/2}$ and (*d*) $z/\delta \approx 0.3$. Near the wall (figure 6*a*), all flows exhibit a similar premultiplied energy spectra, with the inner peak clearly visible at $\lambda_x^+ \approx 1000$. It can be seen that the intensity of the inner peak

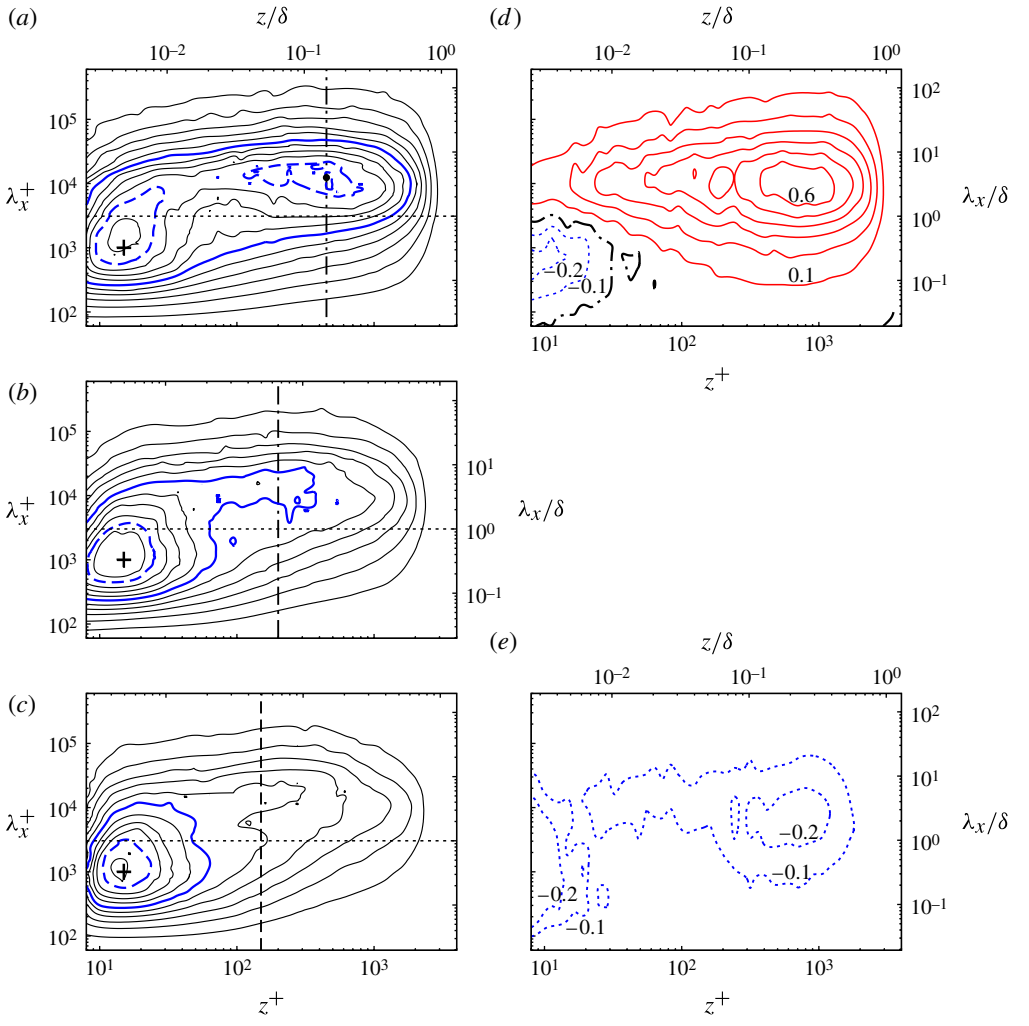

FIGURE 5. (Colour online) (*a–c*) Premultiplied energy spectra of the streamwise velocity $k_x\phi_{uu}/U_\tau^2$. Contour levels are 0.15–1.8 with 0.15 increments. The thicker (blue online) contour corresponds to 0.9 and the dashed (blue online) contour corresponds to 1.5. The symbol '+' denotes the coordinate $z^+ \approx 15$, $\lambda_x^+ \approx 1000$. The vertical lines denote the coordinate $z^+_{AM=0}$. The dotted horizontal line indicates $\lambda_x = \delta$. (*d,e*) Difference between the energy spectra of APG/FPG and ZPG $|k_x\phi^+_{uu}|_{APG/FPG} - |k_x\phi^+_{uu}|_{ZPG}$. Contour levels are from −0.2 to 0.6 in step of 0.1, solid lines indicate positive contours, dashed lines negative contours and dash–dotted lines zero.

is of the same magnitude (within experimental error), suggesting that the small-scale features remain mostly unaffected by the pressure gradient. However, a substantial rise of the energy in the larger wavelengths ($\lambda_x > \delta$) is observed as the pressure gradient increases. This corresponds to a strengthening of the footprint of the large scales (Hutchins & Marusic 2007*a*) as the pressure gradient increases. At $z^+ \approx 100$ (figure 6*b*), large-scale structures are clearly dominating the flow in the APG case. The most energetic structures at this location have $\lambda_x/\delta \approx 6$. In the FPG case, however, the large scales are certainly not as energetic. In fact, the large-scale energetic peak

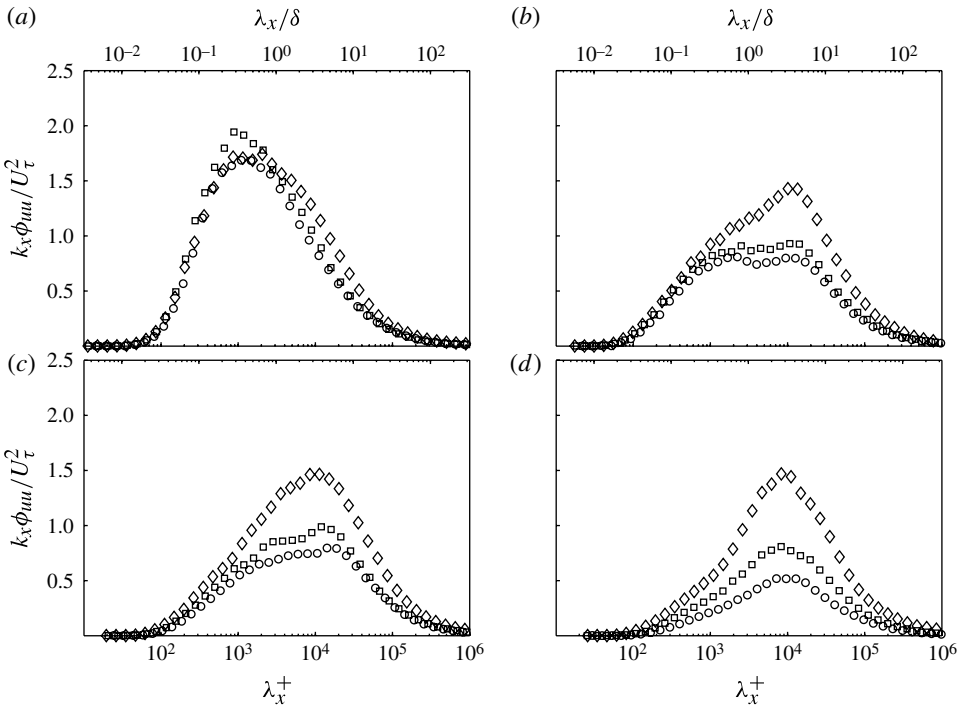

FIGURE 6. Premultiplied energy spectra at four selected wall-normal locations: ♢, APG; □, ZPG; and ○, FPG.

is almost the same magnitude as the small-scale peak. The small-scale structures are observed to be only slightly increased with the changing pressure gradient. In the log-region, at $z^+ \approx 3.9Re_\tau^{1/2}$ (figure 6*c*), the large-scale structures exhibit a peak in ZPG and FPG flows at a wavelength of $\lambda_x/\delta \approx 4$ and $\lambda_x/\delta \approx 5$, respectively. However, in the APG case, the most energetic structures shorten to $\lambda_x/\delta \approx 3$. A similar result was also found by Skåre & Krogstad (1994). This figure confirms that the higher turbulence intensity in the outer region due to pressure gradient increasing (figure 2*b*) comes from the enhanced energy of the large-scale features.

In the outer region at $z/\delta \approx 0.3$ (figure 6*d*), there is clearly more energy in the APG case as compared with the ZPG and FPG cases. The most energetic structures in this region centre at $\lambda_x/\delta \approx 3$, invariant with the pressure gradient. This was somewhat expected after the work of Balakumar & Adrian (2007) and Monty *et al.* (2009) who showed the same result when comparing pipes, channels and ZPG boundary layers. However, the magnitudes of the energy (at any given wavelength) are very different for each pressure gradient, making it difficult to assess the similarities or differences in the distribution of energy across the scales. As a visual aid, it is therefore useful to plot the energy spectra scaled with its maximum magnitude, $(k_x\phi_{uu})_{max}$ as shown in figure 7. This figure clearly shows that the distribution of energy in the far outer region ($z/\delta = 0.3$) is the same for all three pressure gradient cases. This supports the conjecture of Bradshaw (1967*b*) that the large scales can be considered as universal in shape, changing only by velocity and length scale factors. The data here imply that the relevant length scale is the boundary layer thickness, however, the velocity scale is not U_τ (nor U_1 as noted in figure 3). The relevant velocity scale is beyond the scope

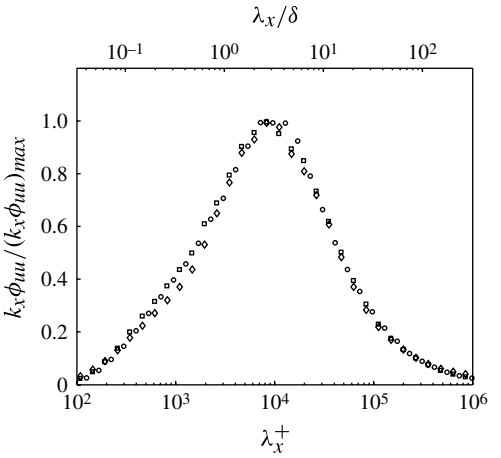

FIGURE 7. Normalized premultiplied energy spectra of streamwise velocity fluctuation at $z/\delta \approx 0.3$: ◇, APG; □, ZPG; and ○, FPG.

of this investigation as data over a greater range of pressure gradients and Reynolds numbers would be required.

Returning to the APG spectra in the log-region (figure 6*c*), the $\lambda_x/\delta \approx 3$ structures, so dominant in the far outer region, also dominate in the log region, such that the $\lambda_x/\delta \approx 6$ peak observed in ZPG boundary layers is overshadowed by these structures. This could be interpreted as meaning superstructures are not shortened by the APG, but rather there are more shorter structures of length $\lambda_x/\delta \approx 3$ in the log region for such pressure gradients.

It is noted that so far a local convection velocity has been used, which may tend to distort the energy of the large scales. Monty *et al.* (2009), del Álamo & Jiménez (2009) and Chung & McKeon (2010) have shown that the large-scale motions move faster than the mean velocity near the wall, such that near-wall spectra obtained by assuming a convection velocity are corrupted by the inappropriate use of the local mean velocity for U_c. Furthermore, it could be argued that the velocity scale of the large eddies should be a velocity representative of the outer region, rather than U_τ. Therefore, the energy spectra from four selected wall-normal locations are reproduced in figure 8 scaled with the free stream velocity and using $U_c = 0.82U_1$ (Dennis & Nickels 2008). In the near-wall region, $z^+ \approx 15$, the energy of the large wavelengths agrees much better between the three pressure gradient cases. This confirms that the large-scale structures do scale with a velocity significantly higher than the friction velocity and convect faster than the local mean. However, U_1 is obviously not a relevant velocity scale for the dominant small-scale motions near the wall. At all other wall-normal locations, the overall picture is essentially the same as in figure 6, except that the large-scale energy differences are reduced. It is noted that a variety of other scalings could have been used (as summarized and analysed by Maciel, Rossignol & Lemay (2006)). The main reason for omitting such analyses is that such scaling arguments are not ideal to identify changes in energy spectra since these scalings are either undefined or unfamiliar in the ZPG case and do not collapse either the high or low wavelengths of the spectrum. In the interest of attempting to understand variations of the APG and FPG relative to the ZPG case, scaling is limited to viscous or outer scaling as presented so far.

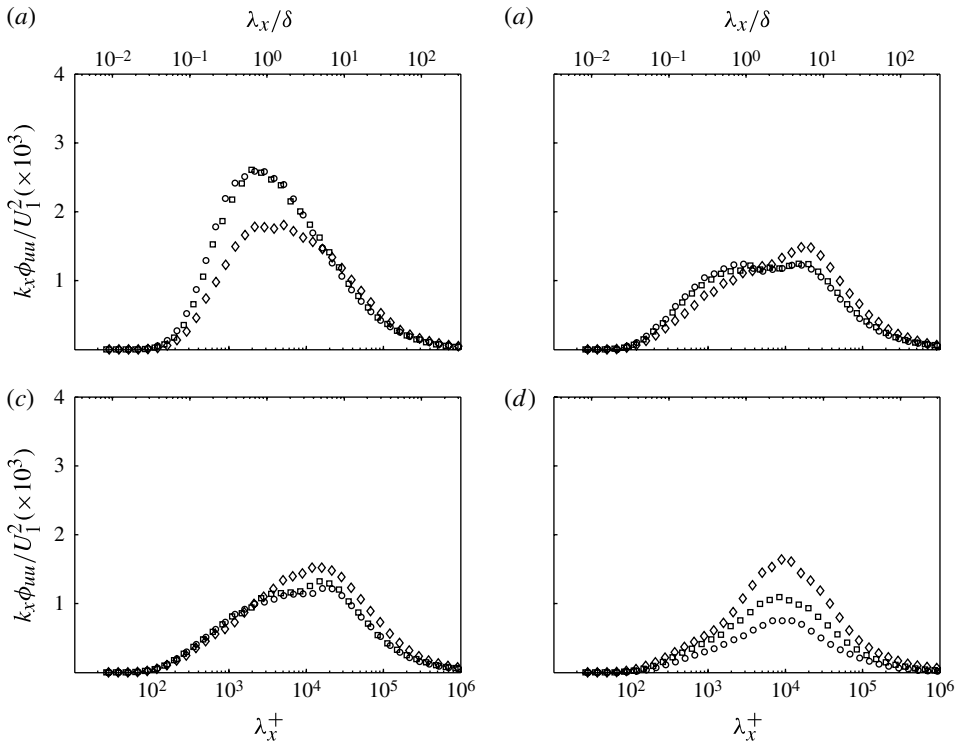

FIGURE 8. Premultiplied energy spectra of streamwise velocity fluctuation $k_x\phi_{uu}/U_1^2$ at selected wall-normal locations: ◊, APG; □, ZPG; and ○, FPG. The temporal spectra are here converted into spatial spectra using Taylor's hypothesis using $\lambda_x = 0.82U_1/f$: (*a*) $z^+ \approx 15$; (*b*) $z^+ \approx 100$; (*c*) $z^+ \approx 3.9Re_\tau^{1/2}$; (*d*) $z/\delta \approx 0.3$.

The energy spectra analysis presented here reveals that the most influenced features in boundary layers subjected to pressure gradient are at the larger scales associated with the outer region. Specifically, large-scale motions are amplified in the APG boundary layer, whereas they are attenuated in the FPG case (relative to the wall friction). Data at a range of mild pressure gradients indicate the phenomena seen here strengthen as the magnitude of the pressure gradient increases; namely, the large-scale energy increases with increasing APG (as noted by Monty *et al.* 2011) and decreases with increasing FPG. These data were omitted for clarity and brevity. The interaction between these large-scale structures and the small-scale structures near the wall is considered in the following section.

3.4. *Scale relationship*

Mathis *et al.* (2009*a*) used a scale decomposition and the Hilbert transformation to develop a tool to quantify the amplitude modulation effect. In that study, it was shown that the near-wall small-scale structures are strongly amplitude modulated by the large-scale motions associated with the log-layer. Furthermore, it was shown that the amplitude modulation effect increases significantly with increasing Reynolds number, which was mainly due to the strengthening of the large-scale features with Reynolds number. Since it is observed here that there are strong differences in the large-scale content when the pressure gradient changes, there are expected consequences for the

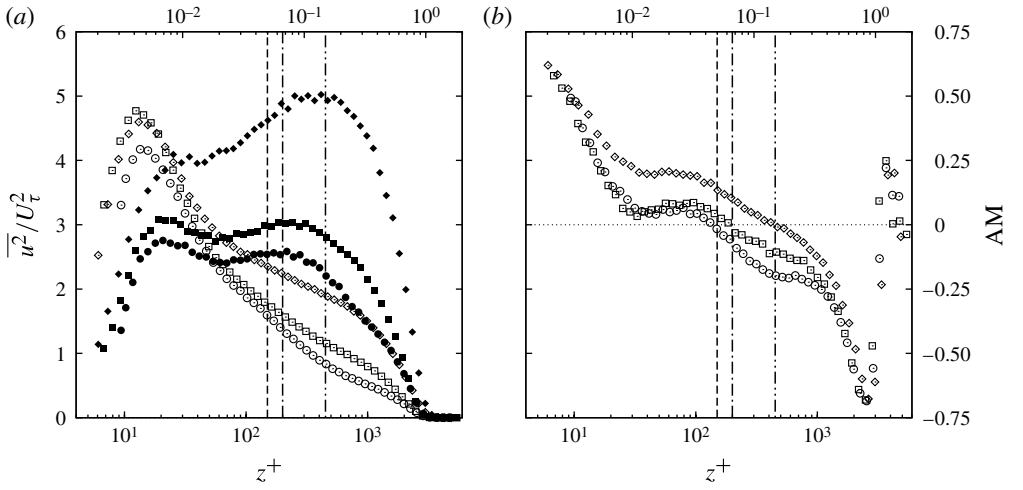

FIGURE 9. (*a*) Decomposition of the broadband turbulent intensity profile $\overline{u^2}/{U_\tau}^2$ into a small- (open symbols) and a large-scale (solid symbols) component. (*b*) Degree of amplitude modulation (AM): ◇, APG; □, ZPG; and ○, FPG. The vertical lines represent the locations of zero amplitude modulation, dashed-dot-dotted line for APG, dash-dotted line for ZPG and dashed line for FPG.

amplitude modulation imparted by the big structures onto the small-scale events. The first step to analyse the scale relationship is to decompose the fluctuating velocity component into a small- and a large-scale component. This is done by applying a cut-off wavelength pass-filter below and above a carefully chosen length scale. As highlighted by Mathis *et al.* (2009*a*,*b*), the cut-off wavelength should always be selected according to the premultiplied energy spectra map. Indeed, the purpose of the scale decomposition is to separate events related to the small-scale motions (e.g. the 'inner-peak' contributors), from large-scale structure events (e.g. the 'outer-peak' contributors). Accordingly, a cut-off length scale $\lambda_x = \delta$ has been chosen. Observing figure 5(*a–c*), this is a suitably located cut-off scale for all three flows, as it appears to best separate the small and large scales.

Figure 9(*a*) shows the small- and large-scale components of the decomposed turbulence intensity profile $\overline{u^2}/{U_\tau}^2$, for all three flows. The small-scale components are represented by the open symbols, while the solid symbols depict the large-scale components. Close to the wall, the small-scale component appears to collapse relatively well around the inner-peak location ($z^+ \approx 15$). It should be emphasized that the observed discrepancy for the FPG case is similar to that observed in the unfiltered intensity profiles, shown in figure 2(*b*). In the outer region, it is observed that the small-scale component becomes more energetic as the pressure gradient increases, which likely is due to the varying shear in the outer region for each flow case. That is, the mean velocity profile is well known to increase in gradient in the wake region as the pressure gradient rises from FPG to APG (see figure 2*a*) and this increased shear should lead to increased small-scale energy. However, the small-scale behaviour is partly attributable to insufficient separation of scales on the scale decomposition. For example, the contours of the outer-energetic peak in figure 5(*a*) extend toward the shorter wavelengths, even below $\lambda_x \approx \delta$. This is more pronounced in the APG case compared with the ZPG and FPG cases. Of course, any

leakage below the cut-off filter will result in increased contributions to the small-scale intensity. Higher-Reynolds-number studies, beyond the capability of our facility, would be required to improve the scale decomposition. Regardless of the decomposition issues, the large-scale component clearly demonstrates that most of the increase in streamwise turbulence intensity (figure 2*b*) is due to the large structures. This is especially notable in the APG boundary layer, where the energy markedly rises in comparison with other flows. It is also observed that the increased energy of the large-scale structures penetrates deep into the boundary layer, with significant large-scale energy augmentation observed close to the wall ($z^+ < 30$). However, the large-scale component shown in figure 2(*a*) is also affected by insufficient scale separation, so higher-Reynolds-number data would be needed to establish the veracity of the double peak observed in figure 2(*a*).

The corresponding degree of amplitude modulation, based on the above scale decomposition, is displayed in figure 9(*b*). All three flows present a similar shape of the degree of amplitude modulation as discussed previously in Mathis *et al.* (2009*a*): a near-wall region highly modulated, with the degree of modulation decreasing toward zero in the log-region and becoming highly negative in the wake region. As stated above, Mathis *et al.* (2009*a*) found that as the Reynolds number of a ZPG boundary layer increases, the large scales become more energetic and consequently increase the amplitude modulation effect. Here, a similar conclusion is made; namely, the large scales are strengthened by increasing the pressure gradient and so is the amplitude modulation. A further observation made by Mathis *et al.* (2009*a*) is that the location of the outer peak in the ZPG boundary layer corresponds to the geometrical centre of the log-layer, $z^+ = 3.9Re_\tau^{1/2}$. This location also coincides with the wall-normal location at which the degree of amplitude modulation crosses zero. In the case of FPG and APG, the criterion of the geometrical centre of the log-region does not hold, as the extent of the logarithmic region is affected by the pressure gradient (it may even disappear in the case of strong APG). However, it is interesting to note that the wall-normal location $z^+_{AM=0}$ in figure 9(*b*) still seems to correspond well to the wall-normal location of the outer peak shown in figure 5. The vertical dash-dotted lines in figure 5(*a–c*) represent the location $z^+_{AM=0}$, which appears to roughly follow the site of the highest energy in the outer region of the spectra map. This observation further supports Bradshaw's idea of the universal structure of the large scales in the outer region, at least in the cases of mild pressure gradients.

As mentioned, the scale separation may not be sufficient at the present Reynolds number ($Re_\tau \approx 3000$) to fully separate the large from the small scales (particularly for the APG boundary layer). Collecting data in all three cases of pressure gradient at equally higher Reynolds number remains a challenging goal. The database analysed here has nevertheless been useful in providing an insight into the interaction between the large and small scales of boundary layers subjected to pressure gradients.

4. Conclusions

A unique comparison of three turbulent boundary layers exposed to three different pressure gradients has been undertaken to identify the similarities and differences in the structure of each flow. To ensure the comparison is valid, each boundary layer evolved from the same nominal initial condition; namely, a ZPG boundary layer with $Re_\tau \approx 2600$.

A statistical analysis showed the usual strengthening of the mean velocity wake as the pressure gradient rose from FPG to APG. The turbulence intensity measurements

were unique in that the non-dimensional sensor length was kept constant such that measurement spatial resolution effects did not corrupt the comparison between experiments. The data showed an increasing intensity throughout the layer, most notably in the outer region. An analysis of the production of turbulence energy showed that it is the combination of mean shear and large-scale activity that leads to this rise in turbulence intensity.

The structure of the flow was investigated through a spectral analysis that revealed an increase in large-scale, outer-region activity as the pressure gradient increased from favourable to adverse. Although there is an overall increase in energy in the far outer region, the distribution of energy (i.e. shape of the spectra) is the same for all flows, suggesting that the large-scale motions have not changed in character, only in number and/or strength.

The modulation of the small scales by the large was found to be affected by the pressure gradient. Owing to the increasing large-scale energy with pressure gradient (from FPG to APG), the modulation effect was found to increase accordingly. That is, there appears to be a stronger near-wall footprint of the large-scale structures in the APG case compared with the ZPG and FPG cases. Interestingly, the wall-normal location of the zero-crossing of the amplitude modulation (the switch from amplification of the small scales to attenuation shown in figure 9*b*) varies significantly with pressure gradient, yet in all cases follows closely the location of the large-scale energetic peak.

Finally, the authors gratefully acknowledge a comment by a reviewer of this article who pointed out that the effects of the pressure gradient on the large-scale energy signature appear to be similar to the effect of the Reynolds number in ZPG turbulent boundary layers (Hutchins & Marusic 2007*a*; Mathis *et al.* 2009*a*). To confirm this would require a challenging investigation at significantly higher Reynolds number, in order to separate both effects.

REFERENCES

ABE, H., KAWAMURA, H. & CHOI, H. 2004 Very large-scale structures and their effects on the wall shear-stress fluctuations in a turbulent channel flow up to $Re_\tau = 640$. *Trans. ASME: J. Fluid Engng* **126**, 835–843.

ADRIAN, R. J. 2007 Hairpin vortex organization in wall turbulence. *Phys. Fluids* **19** (4), 041301.

ADRIAN, R. J., MEINHART, C. D. & TOMKINS, C. D. 2000 Vortex organization in the outer region of a turbulent boundary layer. *J. Fluid Mech.* **422**, 1–53.

DEL ÁLAMO, J. C. & JIMÉNEZ, J. 2003 Spectra of the very large anisotropic scales in turbulent channels. *Phys. Fluids* **15** (6), L41–L44.

DEL ÁLAMO, J. C. & JIMÉNEZ, J. 2006 Linear energy amplification in turbulent channels. *J. Fluid Mech.* **559**, 205–213.

DEL ÁLAMO, J. C. & JIMÉNEZ, J. 2009 Estimation of turbulent convection velocities and corrections to Taylor's approximation. *J. Fluid Mech.* **640**, 5–26.

DEL ÁLAMO, J. C., JIMÉNEZ, J., ZANDONADE, P. & MOSER, R. D. 2004 Scaling of the energy spectra of turbulent channels. *J. Fluid Mech.* **500**, 135–144.

AUBERTINE, C. D. & EATON, J. K. 2005 Turbulence development in a non-equilibrium turbulent boundary layer with mild adverse pressure gradient. *J. Fluid Mech.* **532**, 345–364.

BAILEY, S. C. C., HULTMARK, M., SMITS, A. & SCHULTZ, M. P. 2008 Azimuthal structure of turbulence in high Reynolds number pipe flow. *J. Fluid Mech.* **615**, 121–138.

BALAKUMAR, B. J. & ADRIAN, R. J. 2007 Large and very-large-scale motions in channel and boundary-layer flows. *Phil. Trans. R. Soc.* A **365**, 665–681.

BANDYOPADHYAY, P. R. & HUSSAIN, A. K. M. F. 1984 The coupling between scales in shear flows. *Phys. Fluids* **27** (9), 2221–2228.

BOURASSA, C. & THOMAS, F. O. 2009 An experimental investigation of a highly accelerated turbulent boundary layer. *J. Fluid Mech.* **634**, 359–404.

BRADSHAW, P. 1967*a* Inactive motion and pressure fluctuations in turbulent boundary layers. *J. Fluid Mech.* **30**, 241–258.

BRADSHAW, P. 1967*b* The turbulence structure of equilibrium boundary layers. *J. Fluid Mech.* **29**, 625–645.

CHAUHAN, K., NG, H. C. H. & MARUSIC, I. 2010 Empirical mode decomposition and Hilbert transforms for analysis of oil-film interferograms. *Meas. Sci. Technol.* **21**, 105405, 1–13.

CHUNG, D. & MCKEON, B. J. 2010 Large-eddy simulation of large-scale structures in long channel flow. *J. Fluid Mech.* **661**, 341–364.

DEGRAAFF, D. E. & EATON, J. K. 2000 Reynolds-number scaling of the flat-plate turbulent boundary layer. *J. Fluid Mech.* **422**, 319–346.

DENGEL, P. & FERNHOLZ, H. H. 1990 An experimental investigation of an incompressible turbulent boundary layer in the vicinity of separation. *J. Fluid Mech.* **212**, 615–636.

DENNIS, D. J. C. & NICKELS, T. B. 2008 On the limitations of Taylor's hypothesis in constructing long structures in a turbulent boundary layer. *J. Fluid Mech.* **614**, 197–206.

DIXIT, S. A. & RAMESH, O. N. 2010 Large-scale structures in turbulent and reverse-transitional sink flow boundary layers. *J. Fluid Mech.* **649**, 233–273.

FERNHOLZ, H. H. & WARNACK, D. 1998 The effects of a favourable pressure gradient and of the Reynolds number on an incompressible axisymmetric turbulent boundary layer. Part 1. The turbulent boundary layer. *J. Fluid Mech.* **359**, 329–356.

GANAPATHISUBRAMANI, B., HAMBLETON, N., HUTCHINS, W. T., LONGMIRE, E. K. & MARUSIC, I. 2005 Investigation of large-scale coherence in a turbulent boundary layer using two-point correlation. *J. Fluid Mech.* **524**, 57–80.

GANAPATHISUBRAMANI, B., LONGMIRE, E. K. & MARUSIC, I. 2003 Characteristics of vortex packets in turbulent boundary layers. *J. Fluid Mech.* **478**, 35–46.

GRINVALD, D. & NIKORA, V. 1988 Rechnaya turbulentnost (River Turbulence). Hydrometeoizdat, Russia (in Russian).

HAMBLETON, W. T., HUTCHINS, N. & MARUSIC, I. 2006 Simultaneous orthogonal-plane particular image velocimetry measurements in a turbulent boundary layer. *J. Fluid Mech.* **560**, 53–64.

HUTCHINS, N. & MARUSIC, I. 2007*a* Evidence of very long meandering features in the logarithmic region of turbulent boundary layers. *J. Fluid Mech.* **579**, 1–28.

HUTCHINS, N. & MARUSIC, I. 2007*b* Large-scale influences in near-wall turbulence. *Phil. Trans. R. Soc.* A **365**, 647–664.

HUTCHINS, N., NICKELS, T. B., MARUSIC, I. & CHONG, M. S. 2009 Hot-wire spatial resolution issues in wall-bounded turbulence. *J. Fluid Mech.* **635**, 103–136.

JONES, M. B., MARUSIC, I. & PERRY, A. E. 2001 Evolution and structure of sink flow turbulent boundary layers. *J. Fluid Mech.* **428**, 1–27.

JONES, W. P. & LAUNDER, B. E. 1972 Some properties of sink-flow turbulent boundary layers. *J. Fluid Mech.* **56**, 337–351.

KIM, K. C. & ADRIAN, R. J. 1999 Very large-scale motion in the outer layer. *Phys. Fluids* **11** (2), 417–422.

KLINE, S. J., REYNOLDS, W. C., SCHRAUB, F. A. & RUNSTADLER, P. W. 1967 The structure of turbulent boundary layers. *J. Fluid Mech.* **30**, 741–773.

KROGSTAD, P.-Å & SKÅRE, P. E. 1995 Influence of a strong adverse pressure gradient on the turbulent structure in a boundary layer. *Phys. Fluids* **7**, 2014–2024.

KUNKEL, G. & MARUSIC, I. 2006 Study of the near-wall-turbulent region of the high-Reynolds-number boundary layer using an atmospheric flow. *J. Fluid Mech.* **548**, 375–402.

LEE, J. H. & SUNG, H. J. 2009 Structures in turbulent boundary layers subjected to adverse pressure gradients. *J. Fluid Mech.* **639**, 101–131.

MACIEL, Y., ROSSIGNOL, K.-S. & LEMAY, J. 2006 Self similarity in the outer region of adverse-pressure-gradient turbulent boundary layers. *AIAA J.* **44** (11), 2450–2464.

MARUSIC, I. & HEUER, W. D. C. 2007 Reynolds number invariance of the structure inclination angle in wall turbulence. *Phys. Rev. Lett.* **99**, 41–45.

MARUSIC, I. & HUTCHINS, N. 2007 Study of the log-layer structure in wall turbulence over a very large range of Reynolds number. *Flow Turbul. Combust.* **81**, 115–130.

MARUSIC, I., MATHIS, R. & HUTCHINS, N. 2010 High Reynolds number effects in wall turbulence. *Int. J. Heat Fluid Flow* **31**, 418–428.

MARUSIC, I. & PERRY, A. E. 1995 A wall-wake model for the turbulence structure of boundary layers. Part 2. further experimental support. *J. Fluid Mech.* **298**, 389–407.

MATHIS, R., HUTCHINS, N. & MARUSIC, I. 2009*a* Large-scale amplitude modulation of the small-scale structures in turbulent boudary layers. *J. Fluid Mech.* **628**, 311–337.

MATHIS, R., MONTY, J. P, HUTCHINS, N. & MARUSIC, I. 2009*b* Comparison of large-scale amplitude modulation in turbulent boundary layers, pipes, and channel flows. *Phys. Fluids* **21** (11), 111703.

METZGER, M. M. & KLEWICKI, J. C. 2001 A comparative study of near-wall turbulence in high and low Reynolds number boundary layers. *Phys. Fluids* **13** (3), 692–701.

MONTY, J. P., HARUN, Z. & MARUSIC, I. 2011 A parametric study of adverse pressure gradient turbulent boundary layers. *Int. J. Heat Fluid Flow* **32**, 575–585.

MONTY, J. P., HUTCHINS, N., NG, H. C. H. & CHONG, M. S. 2009 A comparison of turbulent pipe, channel and boundary layer flows. *J. Fluid Mech.* **632**, 431–442.

MONTY, J. P., STEWART, J. A., WILLIAMS, R. C. & CHONG, M. S. 2007 Large-scale features in turbulent pipe and channel flows. *J. Fluid Mech.* **589**, 147–156.

NA, Y. & MOIN, P. 1998 Direct numerical simulation of a separated turbulent boundary layer. *J. Fluid Mech.* **374**, 379–405.

NAGANO, Y., TAGAWA, M. & TSUJI, T. 1992 Effects of adverse pressure gradients on mean flows and turbulence statistics in a boundary layer. In *Proceedings of Turbulent Shear Flows 8*, pp. 7–21Berlin.

NAGANO, Y., TSUJI, T. & HOURA, T. 1998 Structure of turbulent boundary layer subjected to adverse pressure gradient. *Int. J. Heat Fluid Flow* **19**, 563–572.

NAGIB, H. M. & CHAUHAN, K. A. 2008 Variations of von Kármán coefficient in canonical flows. *Phys. Fluids* **20**, 101518.

NICKELS, T. B., MARUSIC, I., HAFEZ, S. & CHONG, M. S. 2005 Evidence of the k_1^{-1} law in a high-Reynolds-number turbulent boundary layer. *Phys. Rev. Lett.* **95**, 074501.

NIKORA, V., NOKES, R., VEALE, W., DAVIDSON, M. & JIRKA, G. H. 2007 Large-scale turbulent structure of uniform shallow free-surface flows. *Environ. Fluid Mech.* **7** (2), 159–172.

PERRY, A. E., MARUSIC, I. & JONES, M. B. 2002 On the streamwise evolution of turbulent boundary layers in arbitrary pressure gradients. *J. Fluid Mech.* **461**, 61–91.

PERRY, A. E., MARUSIC, I. & LI, J. D. 1994 Wall turbulence closure based on classical similarity laws and the attached eddy hypothesis. *Phys. Fluids* **6** (2), 1024.

POPE, S. B. 2000 *Turbulent flows*. Cambridge University Press.

RAHGOZAR, S. & MACIEL, Y. 2011 Low- and high-speed structures in the outer region of an adverse-pressure-gradient turbulent boundary layer. *Experimental Thermal and Fluid Science* **35** (8), 1575–1587.

RAO, K. N., NARASIMHA, R. & BADRI NARAYANAN, M. A. 1971 The 'bursting' phenomena in a turbulent boundary layer. *J. Fluid Mech.* **48**, 339–352.

ROBINSON, S. K. 1991 Coherent motions in the turbulent boundary layer. *Annu. Rev. Fluid Mech.* **23**, 601–639.

SKOTE, M. & HENNINGSON, D. S. 2002 Direct numerical simulation of a seperated turbulent boundary layer. *J. Fluid Mech.* **471**, 107–136.

SKOTE, M., HENNINGSON, D. S. & HENKES, R. A. W. M. 1998 Direct numerical simulation of self-similar turbulent boundary layers in adverse pressure gradients. *Flow Turbulence Combustion* **60**, 47–85.

SKÅRE, P. E. & KROGSTAD, P.-Å. 1994 A turbulent equilibrium boundary layer near separation. *J. Fluid Mech.* **272**, 319–348.

SPALART, P. R. & COLEMAN, G. N. 1997 Numerical study of a separation bubble with heat transfer. *Eur. J. Mech.* B Fluids **16**, 169–189.

SPALART, P. R. & WATMUFF, J. H. 1993 Experimental and numerical study of a turbulent boundary layer with pressure gradient. *J. Fluid Mech.* **249**, 337–371.

TOMKINS, C. D. & ADRIAN, R. J. 2003 Spanwise structure and scale growth in turbulent boundary layers. *J. Fluid Mech.* **490**, 37–74.

TOWNSEND, A. A. 1961 Equilibrium layers and wall turbulence. *J. Fluid Mech.* **11**, 97–120.

TOWNSEND, A. A. 1976 *The structure of turbulent shear flow*, 2nd edn. Cambridge University Press.